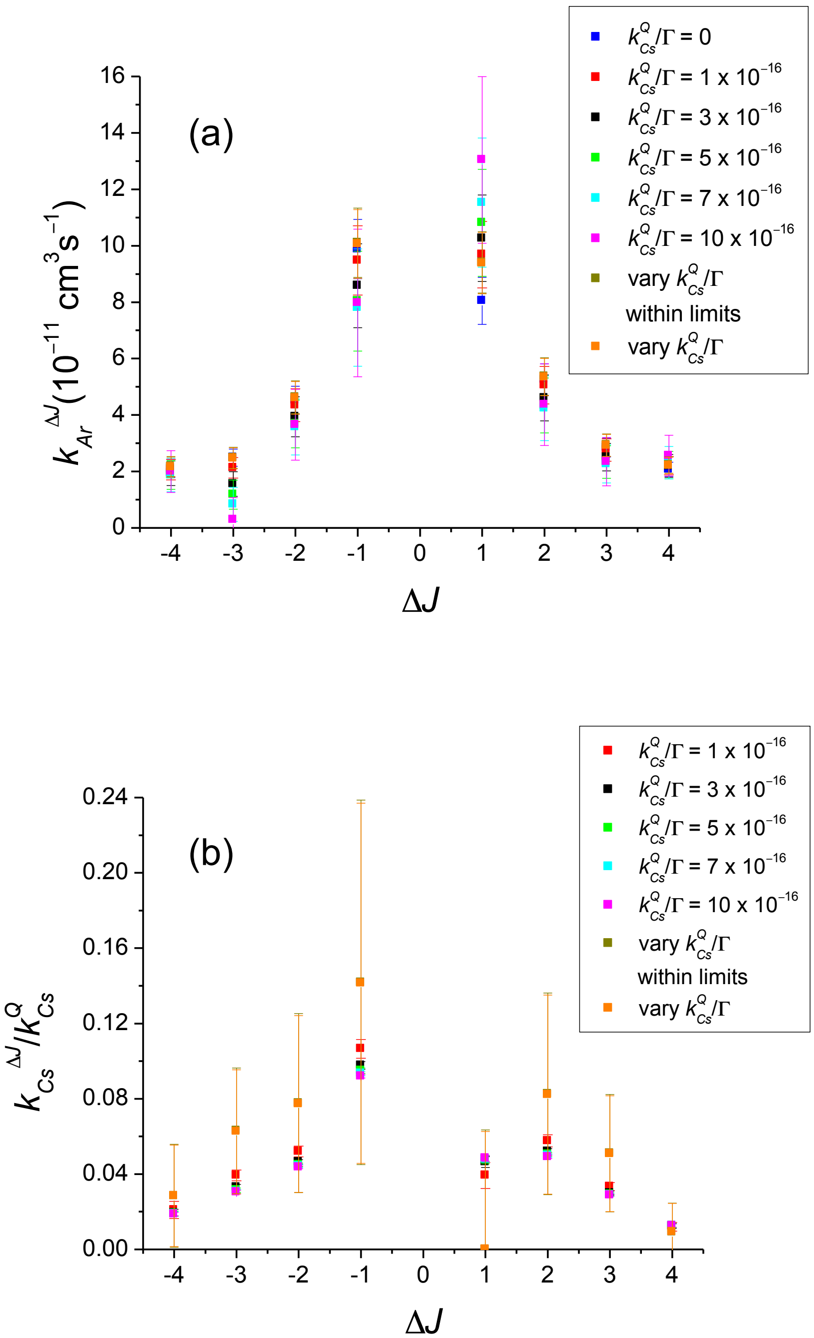

Supplementary Material Fig. 35: (a) Plot of rate coefficients $k_{Ar}^{\Delta J}$ for rotationally inelastic collisions of NaCs $2(A)^1\Sigma^+(v{=}14, J{=}32)$ molecules with argon atoms, comparing the results of fits obtained with various fixed values of k_{Cs}^{Q}/Γ or with k_{Cs}^{Q}/Γ allowed to vary. (b) Plot of rate coefficients for rotationally inelastic collisions of NaCs $2(A)^1\Sigma^+(v{=}14, J{=}32)$ molecules with cesium atoms, in units of the cesium quenching rate coefficient k_{Cs}^{Q}, comparing the results of fits obtained with various fixed values of k_{Cs}^{Q}/Γ or with k_{Cs}^{Q}/Γ allowed to vary. k_{Cs}^{Q}/Γ values are in units of cm^3. For cases listed as "vary k_{Cs}^{Q}/Γ within limits" the range of allowed values was 1×10^{-17} cm^3 < k_{Cs}^{Q}/Γ < 1×10^{-15} cm^3. The value of Γ was taken to be 2.82×10^7 s^{-1}.

R_F vs. n_{Ar} for NaCs $2(A)^1\Sigma^+(v=14, J=32)$, $\Delta J = +1$

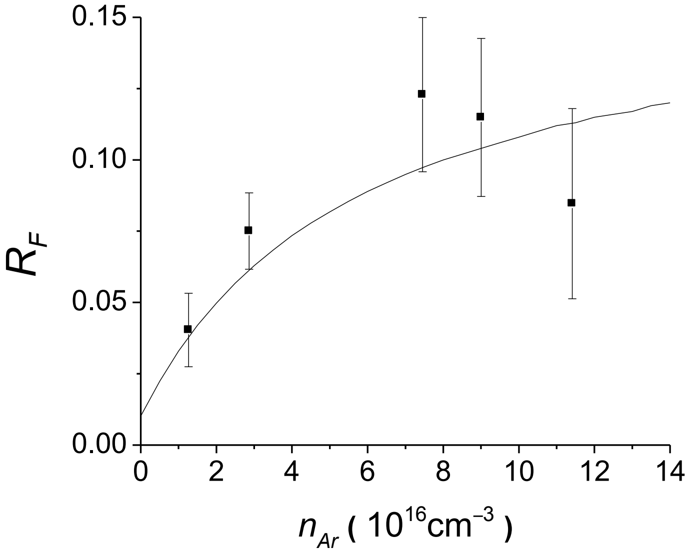

(a) $n_{Cs} = 9.4 \times 10^{14}$ cm^{-3}

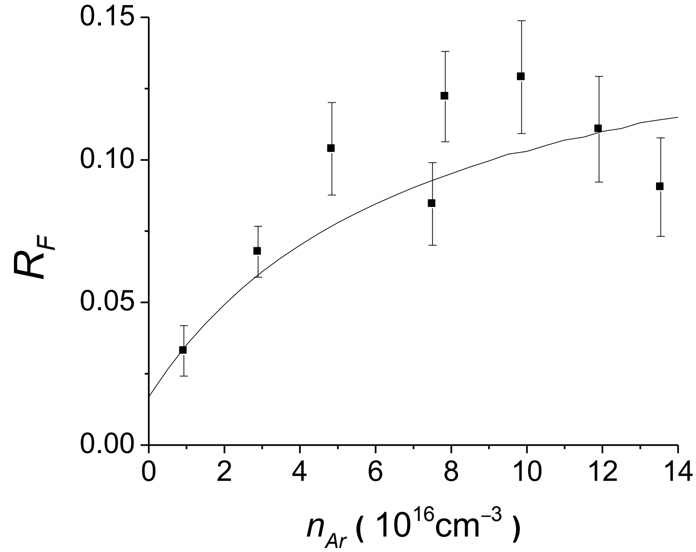

(b) $n_{Cs} = 1.9 \times 10^{15}$ cm^{-3}

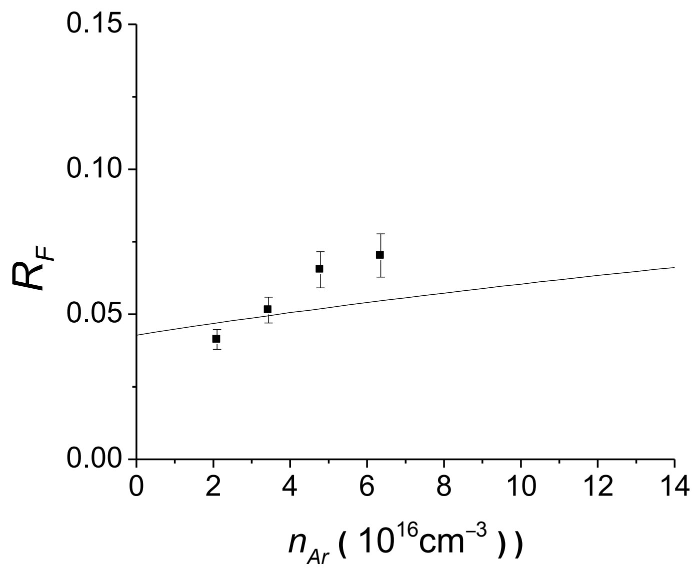

(c) $n_{Cs} = 4.0 \times 10^{16}$ cm^{-3}

Supplementary Material Fig. 36: Plots of fluorescence ratio data (R_F) versus argon density for $\Delta J = +1$ collisions of NaCs $2(A)^1\Sigma^+(v=14, J=32)$ molecules with argon and cesium perturbers. Each panel represents a fixed cesium density n_{Cs}.

R_F vs. n_{Ar} for NaCs $2(A)^1\Sigma^+(v=14, J=32)$, $\Delta J = +2$

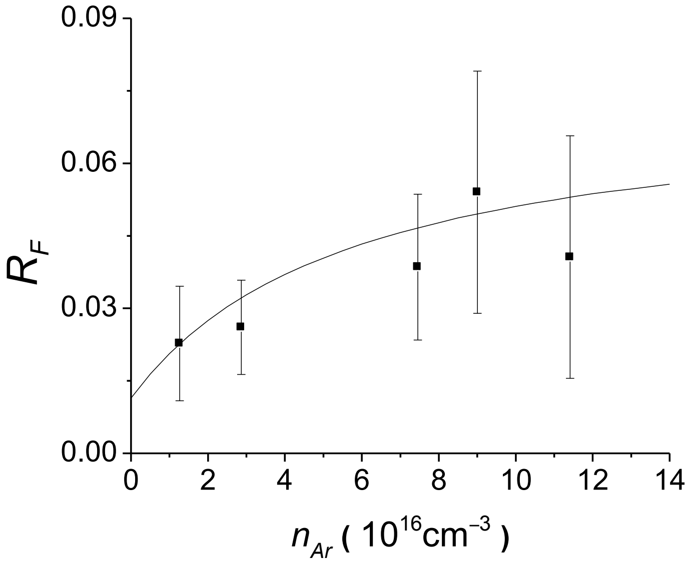

(a) $n_{Cs} = 9.4 \times 10^{14}$ cm^{-3}

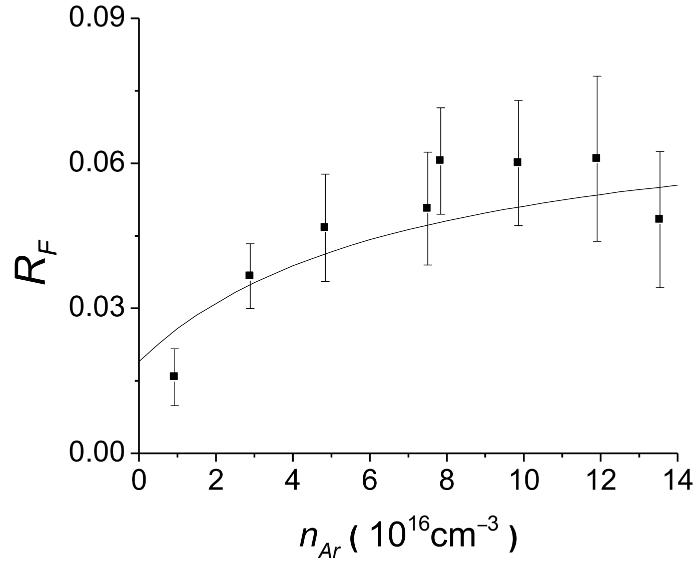

(b) $n_{Cs} = 1.9 \times 10^{15}$ cm^{-3}

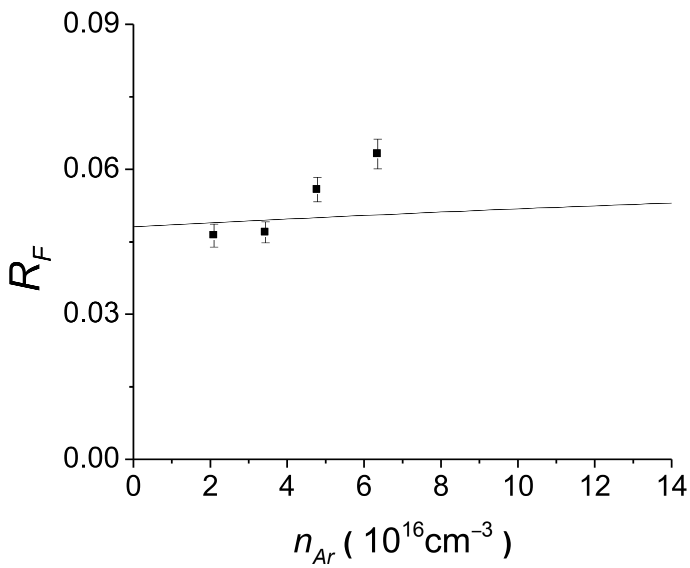

(c) $n_{Cs} = 4.0 \times 10^{16}$ cm^{-3}

Supplementary Material Fig. 37: Plots of fluorescence ratio data (R_F) versus argon density for $\Delta J = +2$ collisions of NaCs $2(A)^1\Sigma^+(v=14, J=32)$ molecules with argon and cesium perturbers. Each panel represents a fixed cesium density n_{Cs}.

R_F vs. n_{Ar} for NaCs $2(A)^1\Sigma^+(v=14, J=32)$, $\Delta J = +3$

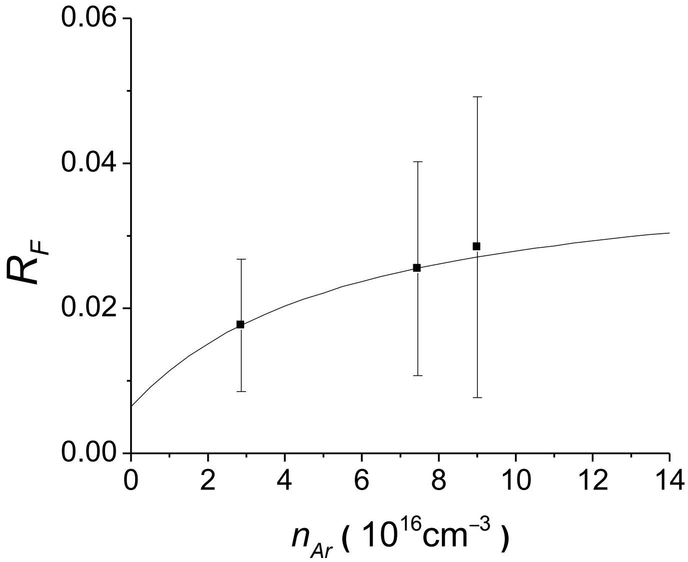

(a) $n_{Cs} = 9.1 \times 10^{14}$ cm^{-3}

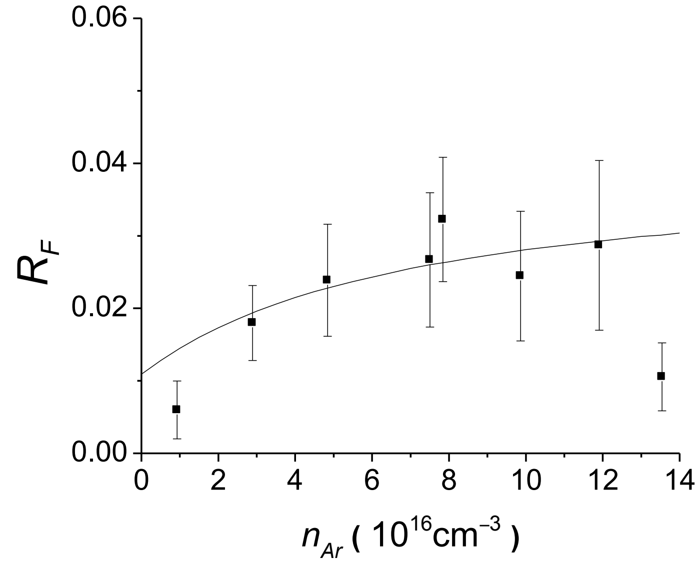

(b) $n_{Cs} = 1.9 \times 10^{15}$ cm^{-3}

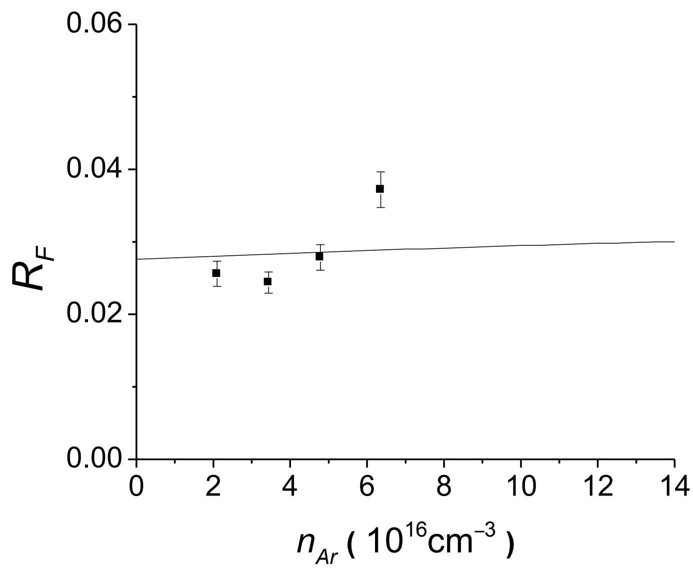

(c) $n_{Cs} = 4.0 \times 10^{16}$ cm^{-3}

Supplementary Material Fig. 38: Plots of fluorescence ratio data (R_F) versus argon density for $\Delta J = +3$ collisions of NaCs $2(A)^1\Sigma^+(v=14, J=32)$ molecules with argon and cesium perturbers. Each panel represents a fixed cesium density n_{Cs}.

R_F vs. n_{Ar} for NaCs $2(A)^1\Sigma^+(v{=}14, J{=}32)$, $\Delta J = +4$

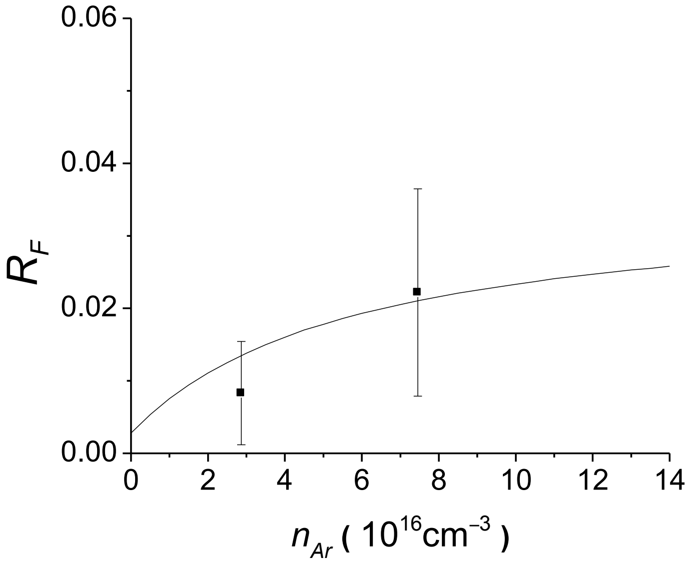

(a) $n_{Cs} = 9.6 \times 10^{14}$ cm^{-3}

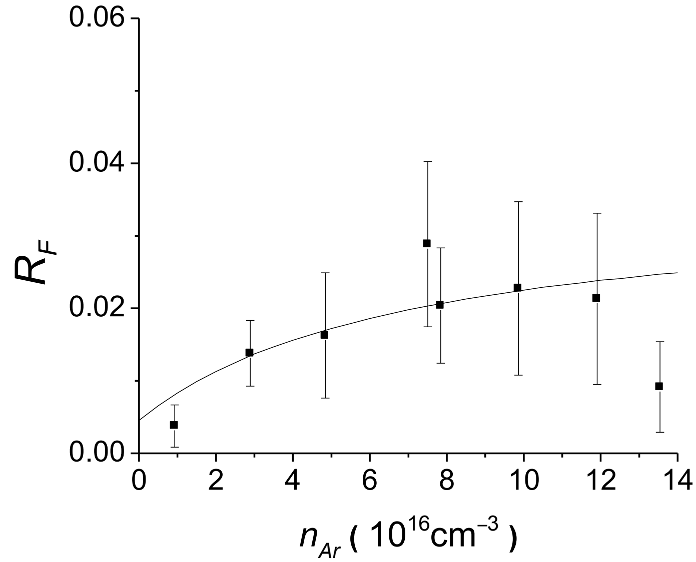

(b) $n_{Cs} = 1.9 \times 10^{15}$ cm^{-3}

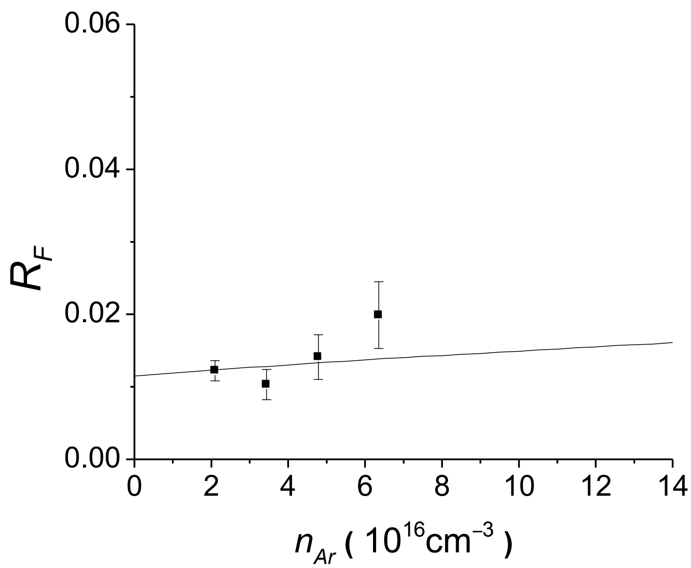

(c) $n_{Cs} = 4.0 \times 10^{16}$ cm^{-3}

Supplementary Material Fig. 39: Plots of fluorescence ratio data (R_F) versus argon density for $\Delta J = +4$ collisions of NaCs $2(A)^1\Sigma^+(v{=}14, J{=}32)$ molecules with argon and cesium perturbers. Each panel represents a fixed cesium density n_{Cs}.

R_F vs. n_{Ar} for NaCs $2(A)^1\Sigma^+(v{=}14, J{=}32)$, $\Delta J = -1$

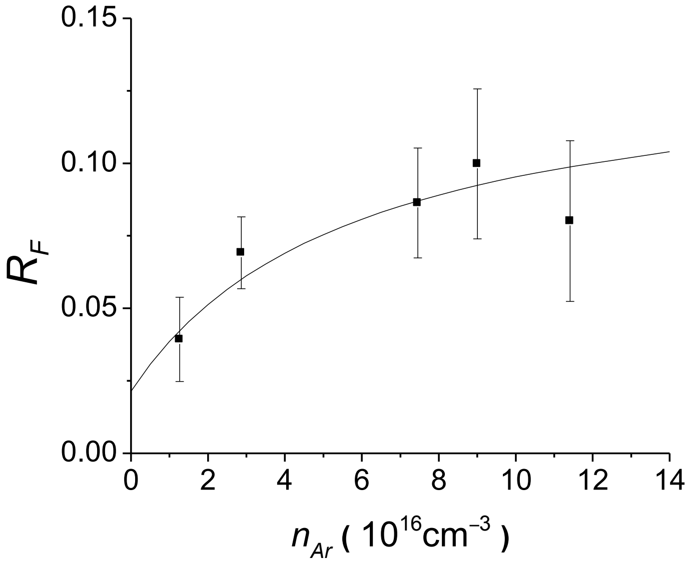

(a) $n_{Cs} = 9.4 \times 10^{14}$ cm^{-3}

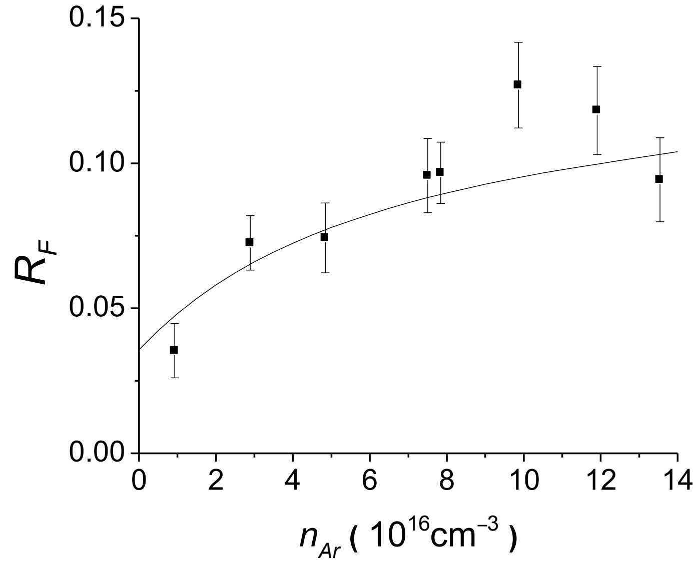

(b) $n_{Cs} = 1.9 \times 10^{15}$ cm^{-3}

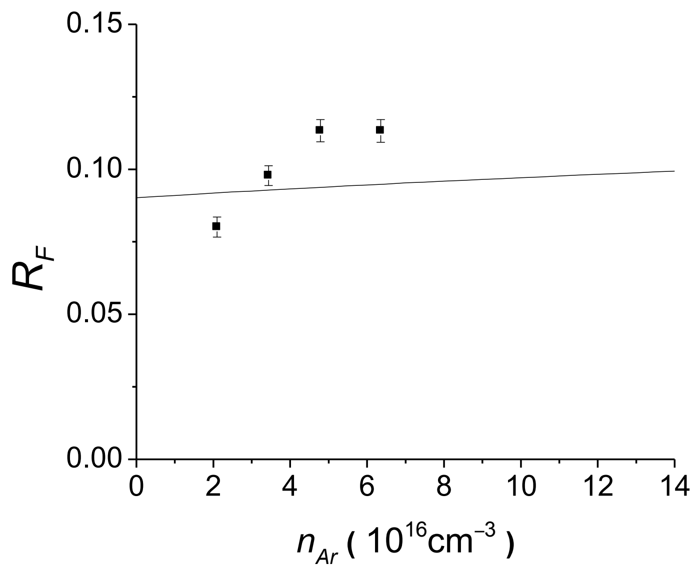

(c) $n_{Cs} = 4.0 \times 10^{16}$ cm^{-3}

Supplementary Material Fig. 40: Plots of fluorescence ratio data (R_F) versus argon density for $\Delta J = -1$ collisions of NaCs $2(A)^1\Sigma^+(v{=}14, J{=}32)$ molecules with argon and cesium perturbers. Each panel represents a fixed cesium density n_{Cs}.

R_F vs. n_{Ar} for NaCs $2(A)^1\Sigma^+(v=14, J=32)$, $\Delta J = -2$

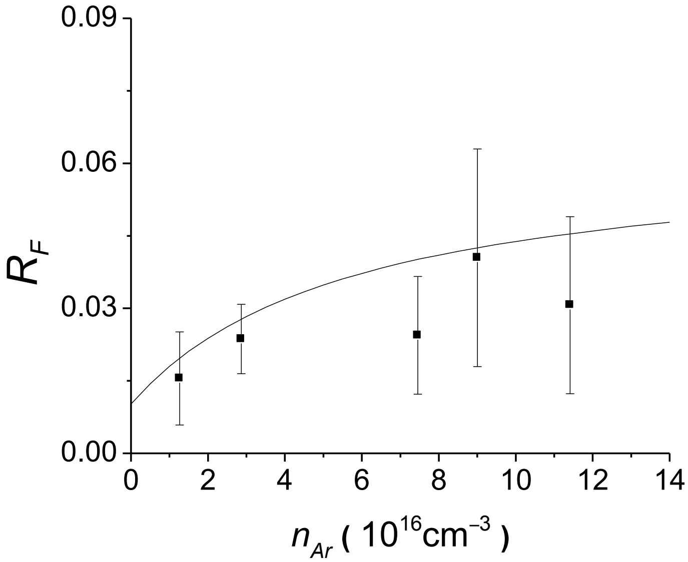

(a) $n_{Cs} = 9.4 \times 10^{14}$ cm^{-3}

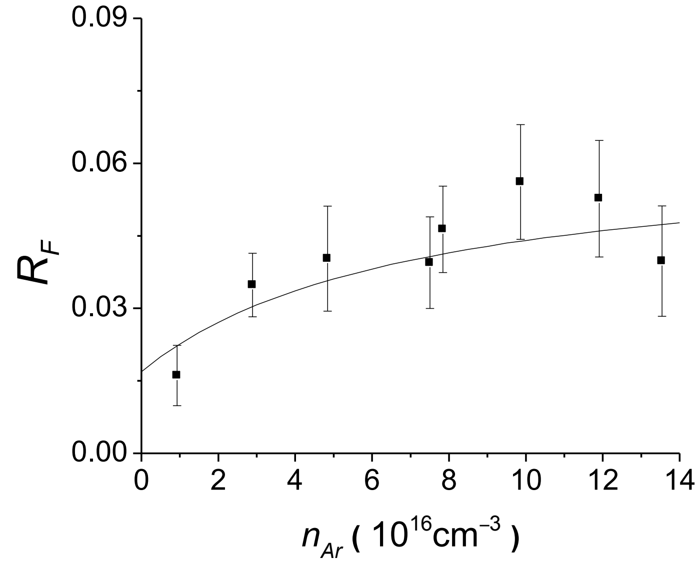

(b) $n_{Cs} = 1.9 \times 10^{15}$ cm^{-3}

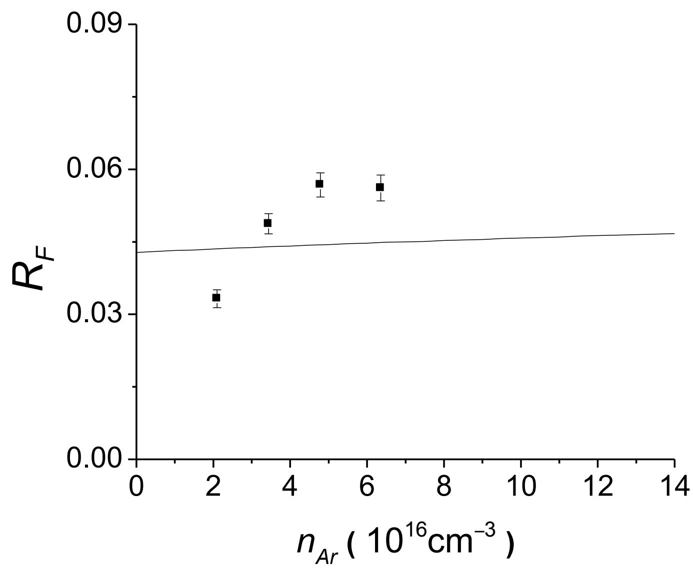

(c) $n_{Cs} = 4.0 \times 10^{16}$ cm^{-3}

Supplementary Material Fig. 41: Plots of fluorescence ratio data (R_F) versus argon density for $\Delta J = -2$ collisions of NaCs $2(A)^1\Sigma^+(v=14, J=32)$ molecules with argon and cesium perturbers. Each panel represents a fixed cesium density n_{Cs}.

R_F vs. n_{Ar} for NaCs $2(A)^1\Sigma^+(v=14, J=32)$, $\Delta J = -3$

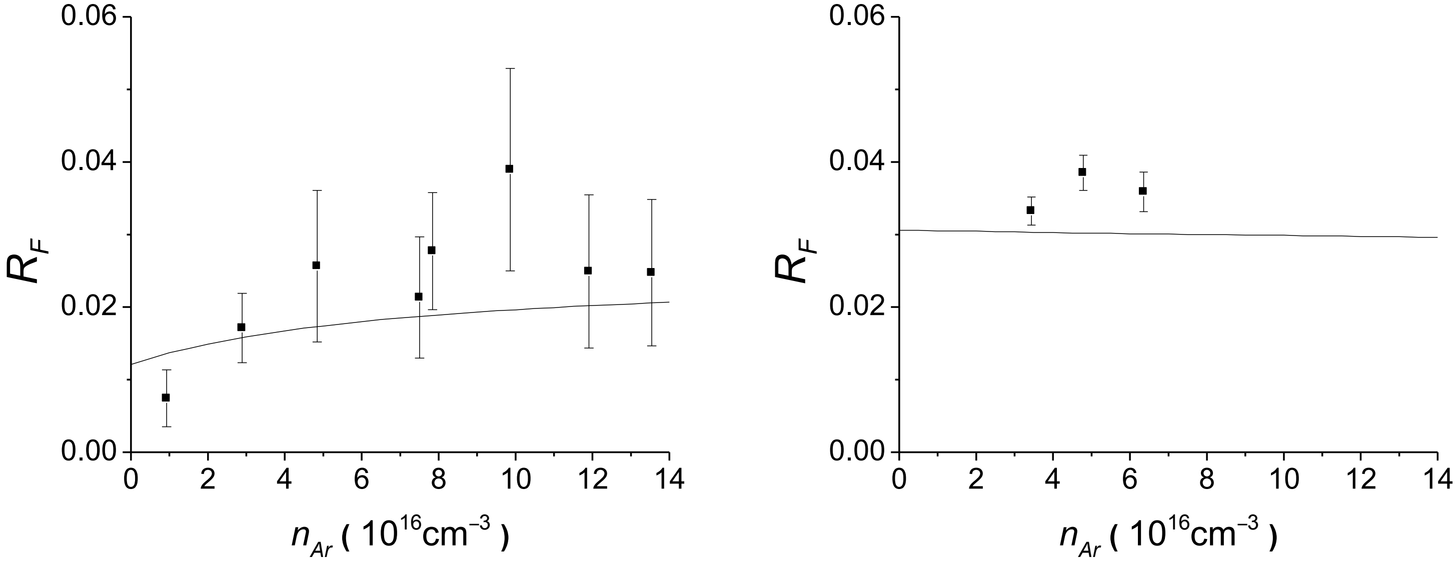

(a) $n_{Cs} = 1.9\times 10^{15}$ cm^{-3} (b) $n_{Cs} = 4.2 \times 10^{16}$ cm^{-3}

Supplementary Material Fig. 42: Plots of fluorescence ratio data (R_F) versus argon density for $\Delta J = -3$ collisions of NaCs $2(A)^1\Sigma^+(v=14, J=32)$ molecules with argon and cesium perturbers. Each panel represents a fixed cesium density n_{Cs}.

R_F vs. n_{Ar} for NaCs $2(A)^1\Sigma^+(v=14, J=32)$, $\Delta J = -4$

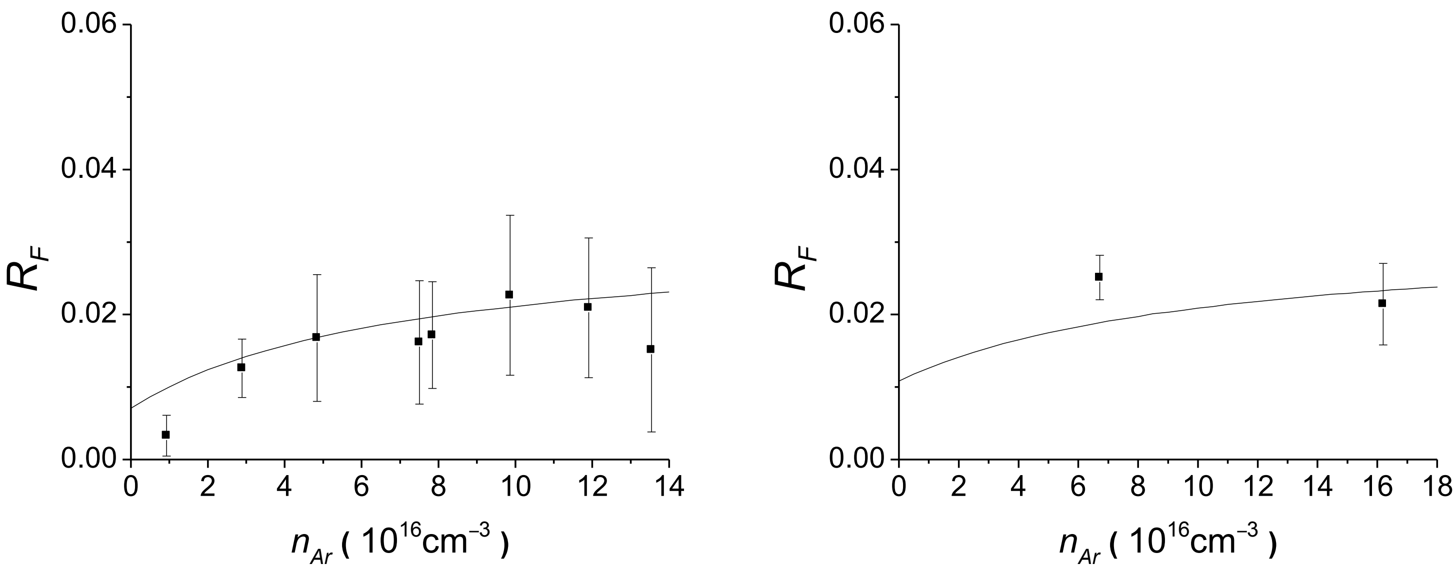

(a) $n_{Cs} = 1.9\times 10^{15}$ cm^{-3} (b) $n_{Cs} = 4.2 \times 10^{15}$ cm^{-3}

Supplementary Material Fig. 43: Plots of fluorescence ratio data (R_F) versus argon density for $\Delta J = -4$ collisions of NaCs $2(A)^1\Sigma^+(v=14, J=32)$ molecules with argon and cesium perturbers. Each panel represents a fixed cesium density n_{Cs}.

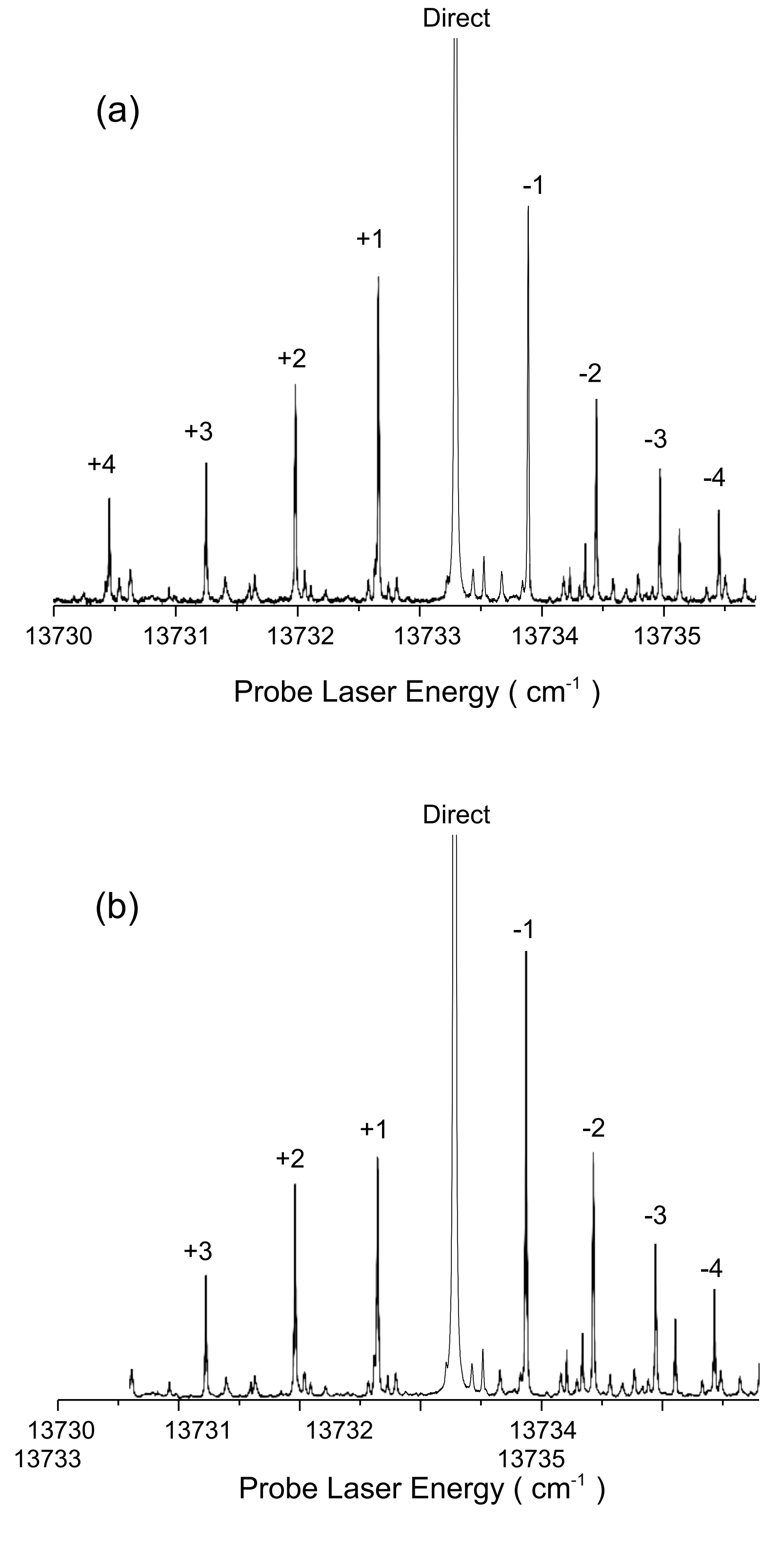

Supplementary Materials Fig. 44: Plot of NaCs excitation spectra for two different cesium densities and similar argon densities ($n_{Ar} \sim 6.0 \times 10^{16}$ cm^{-3}) comparing the difference in relative peak intensities for $\Delta J = +1$ and $\Delta J = -1$ collisional lines. a) $n_{Cs} = 1.04 \times 10^{16}$ cm^{-3}, $I_{col}^{\Delta J=+1} / I_{col}^{\Delta J=-1} = 0.78$. b) $n_{Cs} = 4.37 \times 10^{16}$ cm^{-3}, $I_{col}^{\Delta J=+1} / I_{col}^{\Delta J=-1} = 0.62$.

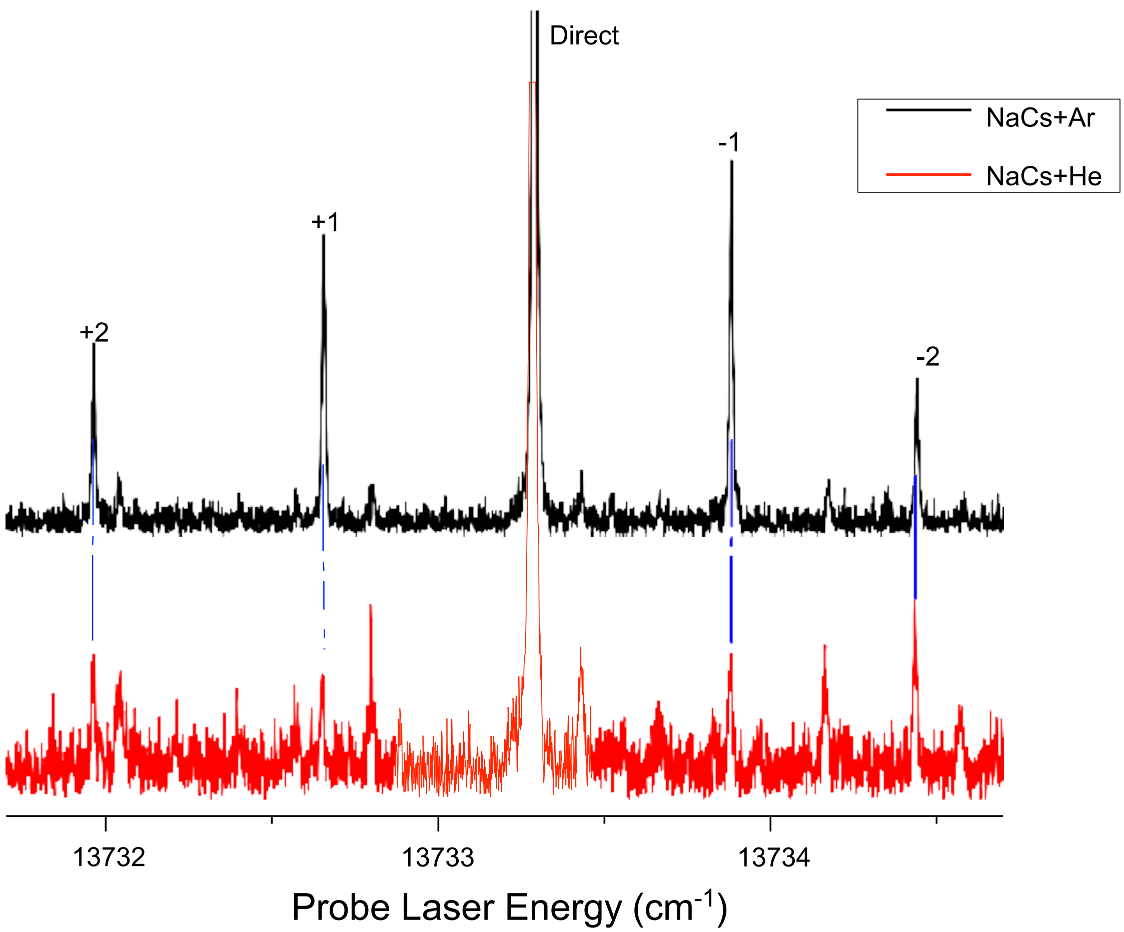

Supplementary Materials Fig. 45: Spectra showing ΔJ = ±1, ±2 NaCs $2(A)^1\Sigma^+(v = 14, J = 32)$ rotationally inelastic collisions with argon and helium buffer gases. The top trace shows a spectrum obtained using argon as the buffer gas, where a decrease in the intensity of the collisional peaks with increasing $|\Delta J|$ can be seen. The bottom trace shows the same NaCs collisional transitions, except with helium as the buffer gas. The number of $\Delta J = \pm 2$ collisions, relative to the number of $\Delta J = \pm 1$ collisions, appears to be greater for helium than for argon perturbers.